This is a postprint version of the following published document:

Ramos, J. J., Merino, M. y Ahedo, E. (2018). Three dimensional fluid-kinetic model of a magnetically guided plasma jet. *Physics of Plasmas,* 25(6).

Three dimensional fluid-kinetic model of a magnetically guided plasma jet

Jesús J. Ramos, Mario Merino,[*] and Eduardo Ahedo[†]

Equipo de Propulsión Espacial y Plasmas (EP2),

Universidad Carlos III de Madrid, Leganés, Spain

A fluid-kinetic model of the collisionless plasma flow in a convergent-divergent magnetic nozzle is presented. The model combines the leading-order Vlasov equation and the fluid continuity and perpendicular momentum equation for magnetized electrons, and the fluid equations for cold ions, which must be solved iteratively to determine the self-consistent plasma response in a three-dimensional magnetic field. The kinetic electron solution identifies three electron populations and provides the plasma density and pressure tensor. The far downstream asymptotic behavior shows the anisotropic cooling of the electron populations. The fluid equations determine the electric potential and the fluid velocities. In the small ion-sound gyroradius case the solution is constructed one magnetic line at a time. In the large ion-sound gyroradius case, ion detachment from magnetic lines makes the problem fully three-dimensional.

[*] mario.merino@uc3m.es

[†] eduardo.ahedo@uc3m.es

I. INTRODUCTION

Applying a convergent-divergent magnetic field to guide the plasma jet of an electric space thruster enables the active control of the thrust magnitude, the thrust direction, and the specific impulse. The contactless operation of such a magnetic nozzle[1–5] (MN) avoids the efficiency, erosion and thermal problems of solid nozzles, and adds propulsive flexibility to address different mission needs. For these reasons, MNs constitute the acceleration stage of several next-generation plasma thrusters, such as the helicon plasma thruster (HPT)[6–14], the electron cyclotron resonance thruster (ECRT)[15–17], the applied-field magnetoplasma-dynamic thruster (AF-MPDT) [18–22], and the variable specific impulse magnetoplasma rocket (VASIMR) [23–25].

Understanding the physics of the plasma beam created by a MN is essential to maximize the magnetic thrust generated by the MN, optimize the thruster performances, and reduce the negative impact of the energetic charged particles from the periphery of the plasma beam on the spacecraft, which takes place mainly if the beam divergence is large. A review of the state-of-art of the knowledge on the physics of propulsive MNs can be found in Ref. [5].

There are several key aspects and related challenges in MN physics. A first one is that the aforementioned thrusters use different heating mechanisms to deliver power to the plasma, resulting in different forms of internal energy, which determines the conversion process into axially directed kinetic energy in the MN. For instance, HPTs store plasma internal energy isotropically on the electrons, ECRT do it anisotropically on electrons, while VASIMR do it anisotropically on ions, and the AF-MPDT seems to store it partially in both populations. In a macroscopic view, isotropic internal energy is converted into axially directed one through electrical and fluid-mechanical (i.e. pressure) forces, while magnetic mirror conversion plays also a role when internal energy is anisotropic.

A second challenge is related to the modeling of the near-collisionless plasma expansion regime in most of the MN, which implies the absence of local thermodynamic equilibrium. This makes uncertain the application of a fluid closure to each species[26], and calls for a description that retains the dominant kinetic effects[27] In the particular case of the electron population, which consists of a majority of confined electrons plus a small tail of energetic free electrons that compensate the emitted ion current, the habitual isothermal

or adiabatic closure relations do not provide an adequate description; while experimentally-fitted polytropic laws[28–30] provide a higher degree of sophistication, they still misrepresent the local electron cooling behavior and the development of anisotropy.

Thirdly, the knowledge of the far plume presents several issues and processes to be assessed. One of them is the total electric potential fall along the MN, which is set by the full expansion of the plasma beam, closely related to the thruster specific impulse and determinant in the interaction between the plasma and the spacecraft wet surfaces. The total potential fall depends again on the electron thermodynamics and also on the ratio of bulk electron current extracted from the plasma source to the thermal electron flux[31, 32]. A second one is the plasma detachment from the MN[33], and thus the effective plume divergence angle. The detachment of the demagnetizing ions downstream due to their inertia is well understood[34], but the picture remains incomplete without a model that allows treating electron demagnetization too.

A fourth challenge is the study of the plasma expansion in a three-dimensional (3D) MN, like the one sketched in Fig. 1. While most MNs are axisymmetric (and plasma and magnetic tubes are well identified), some applications, such as the magnetic control of the thrust vector[35], are based on MNs with variable 3D shape. The extension of the numerical treatment from the two-dimensional (2D) to a 3D nozzle geometry is not straightforward and requires a careful analysis of the most suitable way to integrate the set of equations.

The previous efforts by Ahedo, Merino and coworkers in dealing with MN physics are summarized in [5], and can be divided in three MN model types. Firstly, there is a 2D/3D fully-magnetized and stationary fluid model[36], implemented in the open-source FUMAGNO code[37] with a simple closure relation for the plasma pressures (polytropic or isothermal electrons and quasi-cold ions). The model is useful to analyze the near-region of a divergent MN, where most of the thrust gain takes place, and allowed to demonstrate the feasibility of the magnetic control of the thrust vector with a 3D MN[35]. The model is surprisingly simple, as the fluid equations in the fully-magnetized limit can be integrated along each magnetic line independently.

Secondly, there is a 2D stationary fluid model with partially demagnetized ions and the same simple fluid closure for the isotropic plasma pressures, implemented in the code DIMAGNO[26]. This model is more suitable to the mild magnetic strengths used in most plasma thrusters, and allows studying the far-region plume and ion detachment from the
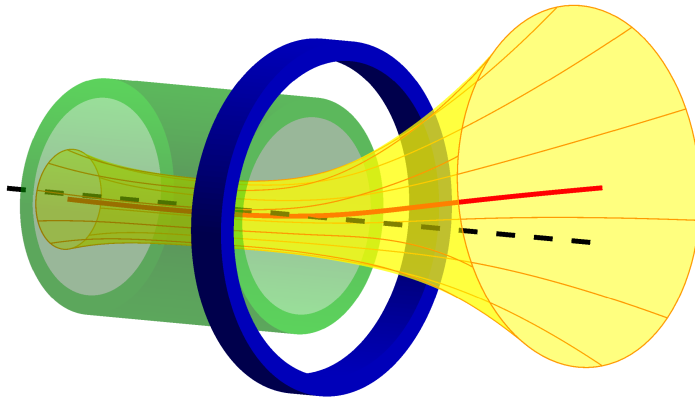
FIG. 1. Sketch of a three-dimensional magnetic field representative of a HPT or ECRT, generated by a solenoid (green) and a 3D MN (blue) composed of 15 deg tilted coils. A single magnetic tube has been plotted (yellow). The central magnetic line (red line) and the axis of symmetry (dashed black line) are shown.

closed magnetic field lines. The model applies efficiently the method of characteristics to integrate the ion equations. Extensions of the core DIMAGNO model have evaluated the effects of collisions[33], electron inertia[38], double-Maxwellian electron populations[39], and plasma-induced magnetic field[40] on the beam expansion.

The phenomenological closure of the electron fluid equations is the weakest aspect of the previous models. The third type of MN models, already developed, is a fully-magnetized, stationary, kinetic, paraxial model, which integrates along the MN axis the Vlasov equation for the velocity distribution function (VDF) of each species[31]. The model demonstrates that collisionless cooling and development of temperature anisotropy are due to the emptying of regions in the VDF space as the plasma beam flows downstream into vacuum. Unfortunately, this kinetic model brings up a new issue: there are islands in the VDF phase space containing trapped electrons, disconnected from the boundary conditions of the problem, so their VDF is unknown. Incidentally, this model is fully analogous to that of an unmagnetized plasma plume[41]. A posterior time-dependent kinetic paraxial model has demonstrated the formation of trapped populations in the transient period of formation of the MN[32].

This paper attempts to continue these previous modeling efforts by establishing a consis-

tent 3D stationary fluid-kinetic model of the MN, which takes advantage when possible of fluid equations and relies on the moments of the collisionless VDF when necessary. Mathematical consistency is achieved by carefully applying the hierarchy of magnitudes established by the relative orders of the main dimensionless parameters. The resulting model unifies two main lines of work and can be used to tackle the issues commented above.

The rest of the article is structured as follows. The fluid-kinetic model is derived in Section II. Section III discusses the integration of the VDF for electrons, raises again the issue of the presence of trapped electrons, and analyzes asymptotically their influence on the downstream asymptotic behavior of the beam. Section IV discusses the fluid model for nearly-cold ions and its coupling with the previous electron kinetic model. Fully-magnetized and partially-magnetized ion cases are distinguished. For the last case, two possible schemes to solve it in 3D are proposed. Section V discusses the posterior determination of electron currents and related issues. Finally, Section VI gathers the conclusions of this work.

II.   FLUID-KINETIC MODEL FOR A MAGNETIC NOZZLE PLASMA

To a good approximation, the plasma in the MN of a space thruster can be assumed to be collisionless and, at least before it becomes too diluted at far distances from the nozzle throat, quasineutral. For each plasma species characterized by particle mass m_s and electric charge e_s, the fluid equations that describe the conservation of particles and momentum are

$$\frac{\partial n_s}{\partial t} + \nabla \cdot (n_s \boldsymbol{u}_s) = 0 \tag{1}$$

and

$$m_s n_s \left[\frac{\partial \boldsymbol{u}_s}{\partial t} + (\boldsymbol{u}_s \cdot \nabla) \boldsymbol{u}_s \right] + \nabla \cdot \mathsf{P}_s - e_s n_s \left(\boldsymbol{E} + \boldsymbol{u}_s \times \boldsymbol{B} \right) = 0, \tag{2}$$

where n_s and $\boldsymbol{u}_s$ are respectively the macroscopic particle density and flow velocity, P_s is the pressure tensor,

$$\mathsf{P}_s(\boldsymbol{x}, t) = m_s \int (\boldsymbol{v} - \boldsymbol{u}_s)(\boldsymbol{v} - \boldsymbol{u}_s) \, f_s(\boldsymbol{x}, \boldsymbol{v}, t) \, \mathrm{d}^3 \boldsymbol{v}, \tag{3}$$

and $f_s(\boldsymbol{x}, \boldsymbol{v}, t)$ is the distribution function that satisfies the collisionless Vlasov equation. For such a collisionless plasma, the mean scalar temperatures can be defined as $T_s \equiv$

$\text{tr}(\mathsf{P}_s)/(3n_s)$. The electromagnetic fields are determined by Ampere's and Faraday's laws,

$$\nabla \times \boldsymbol{B} = \mu_0 \left(\boldsymbol{j}^c + \boldsymbol{j}^p \right), \tag{4}$$

$$\nabla \times \boldsymbol{E} = -\frac{\partial \boldsymbol{B}}{\partial t}, \tag{5}$$

along with $\nabla \cdot \boldsymbol{B} = 0$ and the quasineutrality condition

$$\sum_s e_s n_s = 0. \tag{6}$$

In equation (4), the source for the magnetic field includes the current $\boldsymbol{j}^c$ in the coils that generate the externally applied nozzle field, and the current $\boldsymbol{j}^p = \sum e_s n_s \boldsymbol{u}_s$ in the plasma.

It is advantageous to determine $\boldsymbol{u}_s$ from the macroscopic fluid equations (1), (2) and use the kinetic solution for f_s only to close such collisionless fluid system. To this end, we consider the kinetic equation in the reference frame of the macroscopic flow of the species under consideration, in which the phase-space velocity coordinate is the peculiar velocity $\boldsymbol{w} = \boldsymbol{v} - \boldsymbol{u}_s$. Thus, the expression of the pressure tensor reduces to

$$\mathsf{P}_s(\boldsymbol{x}, t) = m_s \int \boldsymbol{w}\boldsymbol{w} \, f_s(\boldsymbol{x}, \boldsymbol{w}, t) \, \mathrm{d}^3\boldsymbol{w} \tag{7}$$

and the collisionless kinetic equation for $f_s(\boldsymbol{x}, \boldsymbol{w}, t)$ becomes

$$\frac{\partial f_s}{\partial t} + (\boldsymbol{w} + \boldsymbol{u}_s) \cdot \frac{\partial f_s}{\partial \boldsymbol{x}} + \left[\frac{e_s}{m_s}\boldsymbol{w} \times \boldsymbol{B} + \frac{\boldsymbol{F}_s}{m_s n_s} - (\boldsymbol{w} \cdot \nabla)\boldsymbol{u}_s \right] \cdot \frac{\partial f_s}{\partial \boldsymbol{w}} = 0, \tag{8}$$

where

$$\boldsymbol{F}_s = e_s n_s (\boldsymbol{E} + \boldsymbol{u}_s \times \boldsymbol{B}) - m_s n_s \left[\frac{\partial \boldsymbol{u}_s}{\partial t} + (\boldsymbol{u}_s \cdot \nabla)\boldsymbol{u}_s \right] \tag{9}$$

is the force density that combines the electric force in the moving frame with the inertial force that arises from the transformation to such accelerating frame. Using the relationships $\int f_s(\boldsymbol{x}, \boldsymbol{w}, t) \, \mathrm{d}^3\boldsymbol{w} = n_s$ and $\int \boldsymbol{w} \, f_s(\boldsymbol{x}, \boldsymbol{w}, t) \, \mathrm{d}^3\boldsymbol{w} = 0$, the 1 and $\boldsymbol{w}$ moments of equation (8) yield the fluid continuity and momentum conservation equations (1), (2).

In addition to the quasineutral approximation and the neglect of collisions, our theoretical model for the plasma in a space thruster MN will incorporate a number of simplifying idealizations. The electrons will be assumed magnetized, i.e. their Larmor radius of gyration about the magnetic field ρ_e will be assumed much smaller than the characteristic length scale of the system L. The electron mass will be assumed much smaller than the ion

mass, and the ion temperature much smaller than the electron temperature, consistent with a plasma production and heating system based on the interaction of radio-frequency waves with the magnetized electrons as in HPTs and ECRTs. The electron β_e parameter, namely the ratio of electron pressure to magnetic pressure, will be assumed sufficiently small for the plasma current contribution to the magnetic field to be negligible compared to the field externally generated by the hardwired coils. On the other hand and for the sake of simplicity, it will be assumed that the plasma contains a single ion species of unit charge, hence the quasineutrality condition reduces to $n_e = n_i = n$. A steady state will be considered, $\partial/\partial t = 0$, so equation (5) yields $\boldsymbol{E} = -\nabla\phi$, where the electric potential is commensurate with the electron temperature, $e\phi \sim T_e$. No simplifying assumptions will be made regarding the spatial geometry of the system, and a three-dimensional formulation will be maintained, to allow the analysis of non-axisymmetric MNs with thrust vector control[35].

Based on the above theoretical assumptions, the mathematical analysis will carry asymptotic expansions in the following small parameters:

$$\frac{\rho_e}{L} \equiv \frac{m_e^{1/2}T_e^{1/2}}{eBL} \ll 1, \qquad \frac{m_e}{m_i} \ll 1, \qquad \frac{T_i}{T_e} \ll 1, \qquad \beta_e \equiv \frac{nT_e}{B^2} \ll 1. \tag{10}$$

This implies the separation of three velocity scales, namely the ion thermal velocity, the sound velocity and the electron thermal velocity, defined respectively as

$$v_{thi} \equiv \sqrt{\frac{T_i}{m_i}} \ll c_S \equiv \sqrt{\frac{T_e}{m_i}} \ll v_{the} \equiv \sqrt{\frac{T_e}{m_e}}. \tag{11}$$

The final assumption is a sonic scale ordering for the macroscopic flows,

$$|\boldsymbol{u}_e| \sim |\boldsymbol{u}_i| \sim c_S. \tag{12}$$

With the above asymptotic expansion scheme, $e\phi \sim T_e \sim m_i|\boldsymbol{u}_i|^2 \gg T_i$ and $e\phi \sim T_e \gg m_e|\boldsymbol{u}_e|^2$, and the leading-order, steady-state fluid system reduces to the cold-ion, massless-electron limit

$$\nabla \cdot (n\boldsymbol{u}_i) = 0 \tag{13}$$

$$m_i \left[\frac{1}{2}\nabla|\boldsymbol{u}_i|^2 + (\nabla \times \boldsymbol{u}_i) \times \boldsymbol{u}_i \right] + e\left(\nabla\phi - \boldsymbol{u}_i \times \boldsymbol{B}\right) = 0 \tag{14}$$

$$\nabla \cdot (n\boldsymbol{u}_e) = 0 \tag{15}$$

$$\nabla \cdot \mathsf{P}_e - en\left(\nabla\phi - \boldsymbol{u}_e \times \boldsymbol{B}\right) = 0. \tag{16}$$

Besides, the leading-order electron pressure tensor for small electron gyroradius ($\rho_e/L \ll 1$) has the gyrotropic form[42]

$$\mathsf{P}_e = p_{e\parallel}\boldsymbol{bb} + p_{e\perp}(\mathsf{I} - \boldsymbol{bb}), \tag{17}$$

where $\boldsymbol{b} = \boldsymbol{B}/B$ is the magnetic unit vector,

$$p_{e\parallel} = m_e \int w_{\parallel}^2 f_e^{(0)}(w_{\parallel}, w_{\perp}) \, \mathrm{d}^3\boldsymbol{w}, \tag{18}$$

$$p_{e\perp} = \frac{m_e}{2} \int w_{\perp}^2 f_e^{(0)}(w_{\parallel}, w_{\perp}) \, \mathrm{d}^3\boldsymbol{w} \tag{19}$$

and the leading-order distribution function $f_e^{(0)}(w_{\parallel}, w_{\perp})$ is independent of the gyrophase angle. This leading-order distribution function satisfies the zero-Larmor-radius drift-kinetic equation in the reference frame of the electron macroscopic flow[43]:

$$(w_{\parallel}\boldsymbol{b} + \boldsymbol{u}_e) \cdot \frac{\partial f_e^{(0)}}{\partial \boldsymbol{x}} + \left\{\boldsymbol{b} \cdot \left[\frac{e}{m_e}\nabla\phi - (\boldsymbol{u}_e \cdot \nabla)\boldsymbol{u}_e\right] - w_{\parallel}(\boldsymbol{bb}) : (\nabla\boldsymbol{u}_e) - \frac{w_{\perp}^2}{2}\boldsymbol{b} \cdot \nabla \ln B\right\} \frac{\partial f_e^{(0)}}{\partial w_{\parallel}}$$
$$+ \frac{w_{\perp}}{2}\left[(\boldsymbol{bb} - \mathsf{I}) : (\nabla\boldsymbol{u}_e) + w_{\parallel}\boldsymbol{b} \cdot \nabla \ln B\right] \frac{\partial f_e^{(0)}}{\partial w_{\perp}} = 0. \tag{20}$$

For the assumed situation where the electron flow velocity is much smaller than the electron thermal velocity ($|\boldsymbol{u}_e| \ll v_{the}$), and for the purpose of evaluating the leading-order moments (18), (19), it is sufficient to solve the small-flow-velocity limit of the above drift-kinetic equation,

$$w_{\parallel}\boldsymbol{b} \cdot \frac{\partial f_e^{(0)}}{\partial \boldsymbol{x}} + \left[\frac{e}{m_e}\boldsymbol{b} \cdot \nabla\phi - \frac{w_{\perp}^2}{2}\boldsymbol{b} \cdot \nabla \ln B\right] \frac{\partial f_e^{(0)}}{\partial w_{\parallel}} + \frac{w_{\perp}w_{\parallel}}{2}\boldsymbol{b} \cdot \nabla \ln B\frac{\partial f_e^{(0)}}{\partial w_{\perp}} = 0. \tag{21}$$

Here, the phase-space advection operator acting on $f_e^{(0)}$ has definite (odd) parity with respect to $w_{\parallel}$. Therefore, the solution for $f_e^{(0)}$ is the sum of two independent solutions, one that is even with respect to $w_{\parallel}$ and another that is odd. Only the even solution is needed in order to evaluate the moments $n(\boldsymbol{x})$ and $\mathsf{P}_e(\boldsymbol{x})$ of interest to close the system of fluid equations (13)–(16).

In order to solve the drift-kinetic equation (21), it is useful to make the change of phase-space coordinates from $(\boldsymbol{x}, w_{\parallel}, w_{\perp})$ to $(\boldsymbol{x}, H, \mu)$, where H and μ are the energy and the magnetic moment,

$$H = \frac{m_e}{2}(w_{\parallel}^2 + w_{\perp}^2) - e\phi(\boldsymbol{x}), \qquad \mu = \frac{m_e w_{\perp}^2}{2B(\boldsymbol{x})} \tag{22}$$

8

and call

$$F(\boldsymbol{x}, H, \mu) = m_e^{-3/2} f_e^{(0)even}(\boldsymbol{x}, w_\parallel, w_\perp). \tag{23}$$

With this change of coordinates we have

$$\boldsymbol{b} \cdot \left.\frac{\partial}{\partial \boldsymbol{x}}\right|_{w_\parallel, w_\perp} = \boldsymbol{b} \cdot \left.\frac{\partial}{\partial \boldsymbol{x}}\right|_{H,\mu} - e(\boldsymbol{b} \cdot \nabla\phi)\frac{\partial}{\partial H} - (\boldsymbol{b} \cdot \nabla \ln B)\mu\frac{\partial}{\partial \mu}, \tag{24}$$

$$\frac{\partial}{\partial w_\parallel} = m_e w_\parallel \frac{\partial}{\partial H}, \tag{25}$$

$$\frac{\partial}{\partial w_\perp} = m_e w_\perp \frac{\partial}{\partial H} + \frac{2\mu}{w_\perp}\frac{\partial}{\partial \mu}, \tag{26}$$

and equation (21) becomes

$$w_\parallel \boldsymbol{b} \cdot \left.\frac{\partial F}{\partial \boldsymbol{x}}\right|_{H,\mu} = 0 \tag{27}$$

which can be solved independently along each magnetic field line, with $\boldsymbol{b} \cdot \partial/\partial\boldsymbol{x}|_{\mu,H} = \partial/\partial\ell|_{H,\mu}$ where ℓ is the arc length. Equation (27) states that for each (H,μ), F is piece-wise constant along ℓ, with discontinuities at the turning points for that family of electrons, i.e. where $w_\parallel = 0$. For a given H and ℓ the range of the magnetic moment is $0 < \mu < \mu_{\max}(\ell, H)$, where

$$\mu_{\max}(\ell, H) = \frac{H + e\phi(\ell)}{B(\ell)} \tag{28}$$

corresponds to $w_\parallel = 0$ from equation (22).

In terms of the (H, μ) variables, the moments of the electron distribution function needed to close the system of fluid equations are:

$$n = 2^{3/2}\pi B \int_{-e\phi}^{\infty} \mathrm{d}H \int_0^{\mu_{\max}} \frac{F\mathrm{d}\mu}{(H + e\phi - \mu B)^{1/2}}, \tag{29}$$

$$p_{e\parallel} = 2^{5/2}\pi B \int_{-e\phi}^{\infty} \mathrm{d}H \int_0^{\mu_{\max}} (H + e\phi - \mu B)^{1/2} F\mathrm{d}\mu, \tag{30}$$

$$p_{e\perp} = 2^{3/2}\pi B^2 \int_{-e\phi}^{\infty} \mathrm{d}H \int_0^{\mu_{\max}} \frac{\mu F\mathrm{d}\mu}{(H + e\phi - \mu B)^{1/2}}. \tag{31}$$

The leading-order drift-kinetic equation (27) for $F(\boldsymbol{x}, H, \mu)$ implies that the parallel gradient of (30) is

$$\boldsymbol{b} \cdot \nabla p_{e\parallel} = p_{e\parallel}(\boldsymbol{b} \cdot \nabla \ln B) + 2^{3/2}\pi B \int_{-e\phi}^{\infty} \mathrm{d}H \int_0^{\mu_{\max}} \frac{(e\boldsymbol{b} \cdot \nabla\phi - \mu\boldsymbol{b} \cdot \nabla B)F\mathrm{d}\mu}{(H + e\phi - \mu B)^{1/2}} \tag{32}$$

and, recalling (29) and (31), this can be expressed as

$$\boldsymbol{b} \cdot \nabla p_{e\parallel} = (p_{e\parallel} - p_{e\perp})(\boldsymbol{b} \cdot \nabla \ln B) + en\boldsymbol{b} \cdot \nabla \phi \qquad (33)$$

which is the parallel component of the electron momentum conservation equation (16). On the other hand, the perpendicular components of (16) and the electron continuity equation (15) do not follow from the leading-order drift-kinetic system (27)–(31) and contain additional information.

In summary, our fluid-kinetic model can be regarded as composed of three subsystems of equations. The first one is the ion fluid system (13), (14) which, assuming the density n to be known, would determine the ion flow velocity $\boldsymbol{u}_i$ and the electric potential ϕ. The second one is the electron drift-kinetic system (27)–(31) which, assuming ϕ to be known, would determine the electron distribution function $F(\boldsymbol{x}, H, \mu)$ and its moments n, $p_{e\parallel}$ and $p_{e\perp}$. The third one is the electron fluid system which includes (15) and the perpendicular components of (16) and that, once the density and the electron pressure tensor are known, determines the three components of the electron flow velocity $\boldsymbol{u}_e$. The first two subsystems must be solved simultaneously for n, ϕ and $\boldsymbol{u}_i$, but the third one for $\boldsymbol{u}_e$ and $p_{e\parallel}$ and $p_{e\perp}$ can be solved alone, after a closed solution of the first two coupled subsystems has been obtained. The magnetic field $\boldsymbol{B}$ is assumed to be fixed and determined by the hardwired coil sources and/or permanent magnets, neglecting the contribution of the plasma current.

We should note that equation (27) admits as integration constants arbitrary functions of (H, μ) that are uniform along the magnetic field lines. These integration constants, which are necessary to define a complete steady-state solution, are partially specified by boundary conditions on the electron distribution function at the upstream and downstream ends of the plasma domain, as will be discussed in more detail in the next Section.

III. ELECTRON DRIFT-KINETIC EQUATION ANALYSIS

The steady-state, zero-Larmor-radius electron drift-kinetic equation (27) for F applies independently to each magnetic field line, in a three-dimensional phase space with coordinates (ℓ, H, μ). The range of the magnetic moment in this phase-space is limited by $0 < \mu < \mu_{\max}(\ell, H)$, where $\mu_{\max}(\ell, H)$ is the surface of electron turning points given by (28). The qualitative shape of the $\mu_{\max}(\ell, H)$ surface can be inferred from the expected variation

of $B(\ell)$ and $\phi(\ell)$ along the magnetic line. As sketched in Fig. 2, in a MN configuration the magnitude of the magnetic field has a maximum at the nozzle throat, and decays to zero at far distances upstream and downstream. Setting the origin of the electric potential at the far upstream side of the nozzle, $\phi(\ell \to -\infty) = 0$, we expect $\phi(\ell)$ to decrease monotonically along the expansion and approach a downstream value $\phi_\infty \equiv \phi(\ell \to +\infty) < 0$ asymptotically. Then, the shape of the $\mu_{\max}(\ell, H)$ surface presents three behaviors, sketched in Fig. 3:

1. For H less than some value $H_* < -e\phi_\infty$, $\mu_{\max}$ is a monotonic function of ℓ, decreasing from $\mu_{\max} = +\infty$ at $\ell = -\infty$ to $\mu_{\max} = 0$ at the value of ℓ that makes $H = -e\phi(\ell)$.

2. For $H_* < H < -e\phi_\infty$, $\mu_{\max}$ decreases with ℓ from $\ell = -\infty$ until some critical value $\ell = \ell_c(H)$ where it reaches a local minimum $\mu_c(H)$, then increases until reaching a local maximum after which it decreases to 0 at the value of ℓ that makes $H = -e\phi(\ell)$.

3. Finally, for $H > -e\phi_\infty$, $\mu_{\max}$ has a minimum value $\mu_c(H)$ at $\ell = \ell_c(H)$ and tends to $+\infty$ as $\ell \to \pm\infty$.

The general solution of the drift-kinetic equation (27) is any function of (H, μ) that is constant along each magnetic line. However, the permitted (ℓ, H, μ) phase-space is made of the different domains discussed above, that are not always connected by the magnetic line. Therefore, the $F(H, \mu)$ solution may be specified differently in each of those domains, which results in the following expression for the general solution of the electron drift-kinetic equation:

$$
\begin{aligned}
F(\ell, H, \mu) &= F_1(H, \mu) & &\text{for } H \leq H_* \\
F(\ell, H, \mu) &= F_{2a}(H, \mu) & &\text{for } H_* < H < -e\phi_\infty, \quad \mu \leq \mu_c(H) \\
F(\ell, H, \mu) &= F_{2b}(H, \mu) & &\text{for } H_* < H < -e\phi_\infty, \quad \mu > \mu_c(H), \quad \ell < \ell_c(H) \\
F(\ell, H, \mu) &= F_{2c}(H, \mu) & &\text{for } H_* < H < -e\phi_\infty, \quad \mu > \mu_c(H), \quad \ell > \ell_c(H) \quad (34) \\
F(\ell, H, \mu) &= F_{3a}(H, \mu) & &\text{for } H \geq -e\phi_\infty, \quad \mu \leq \mu_c(H) \\
F(\ell, H, \mu) &= F_{3b}(H, \mu) & &\text{for } H \geq -e\phi_\infty, \quad \mu > \mu_c(H), \quad \ell < \ell_c(H) \\
F(\ell, H, \mu) &= F_{3c}(H, \mu) & &\text{for } H \geq -e\phi_\infty, \quad \mu > \mu_c(H), \quad \ell > \ell_c(H).
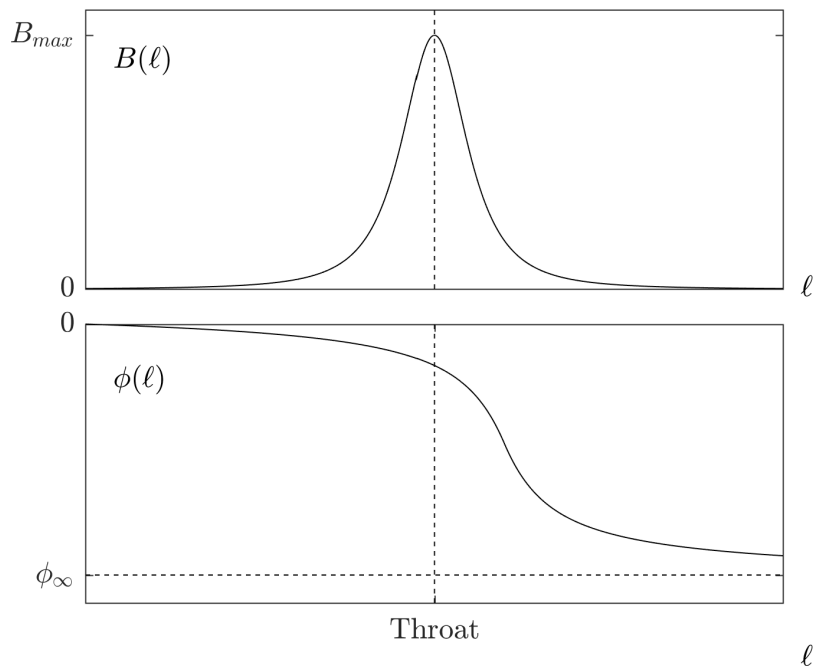\end{aligned}
$$

FIG. 2. Sketch of the magnetic field strength $B(\ell)$ and the electric potential $\phi(\ell)$ along a single magnetic line. The maximum of the magnetic field defines the throat of the flux tube. The electric potential goes to an asymptotic value downstream ϕ_∞.

Next, steady-state boundary conditions are imposed to F. Following [31], the far upstream side of the nozzle is connected to a plasma source characterized by a certain distribution $F_0(H, \mu)$, whereas on the far downstream side all electrons are lost. The domains labeled 1, 2a, 2b, and 3b contain electrons that are connected to the upstream reservoir and are reflected by the combined barrier of the electric potential and the magnetic mirror force. Thus, the steady-state solution in these "reflected-electron" domains should be[31]

$$F_1 = F_{2a} = F_{2b} = F_{3b} = F_0(H, \mu) \tag{35}$$

The domain labeled 3a contains electrons that are connected to the upstream reservoir but are not reflected by the electric and magnetic mirror forces and travel freely to the far downstream side. The steady state distribution function in this "free-electron" domain should be $F_0(H, \mu)$ for positive parallel velocities and zero for negative parallel velocities [31], so their zeroth-order even representation is
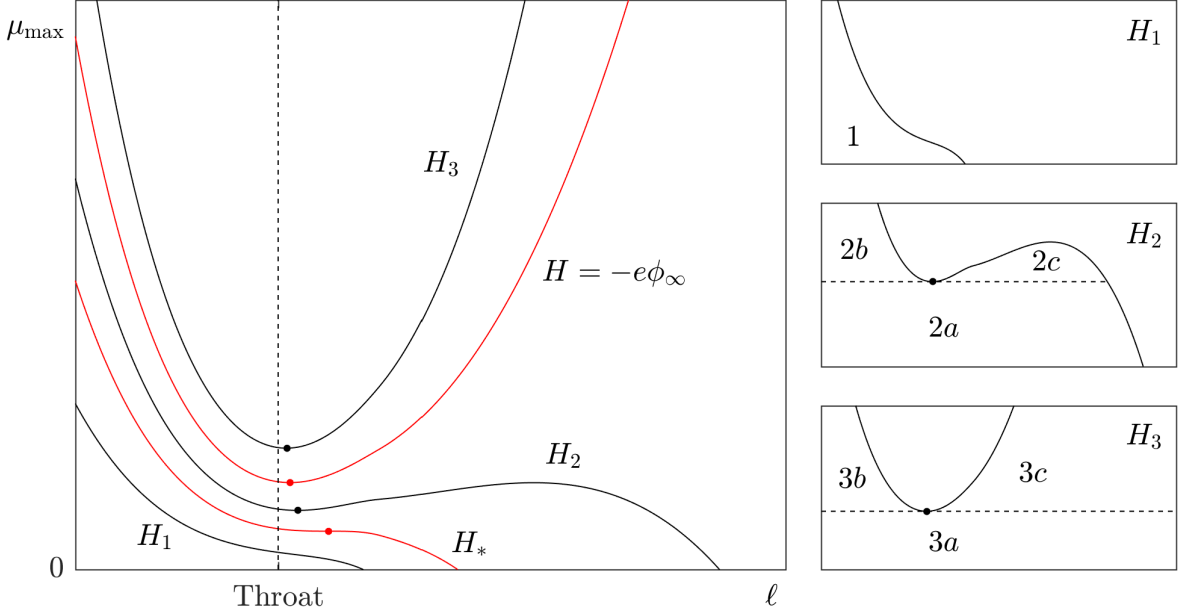
$$F_{3a} = \frac{1}{2} F_0(H, \mu). \tag{36}$$

FIG. 3. Sketch of the $\mu_{\max}(\ell, H)$ function of equation (28) for five increasing values of H: H_1, H_*, H_2, $-e\phi_\infty$, and H_3. Dots denote the position of the minimum of each curve, (ℓ_c, μ_c). The smaller diagrams to the right identify the regions 1, 2a, 2b, 2c, 3a, 3b, 3c of (34) for H_1, H_2, H_3.

The domain labeled 3c is in the shadow of the potential barrier, extending to the far downstream side but not connected to the upstream reservoir, therefore it should be empty in steady-state,

$$F_{3c} = 0. \tag{37}$$

Finally, the domain labeled 2c is a region of trapped electrons where the sampled extent of magnetic line is limited by two particle reflecting points and extends neither to $-\infty$ nor to $+\infty$. There is no physical criterion in the framework of the present model for what the steady-state distribution function should be in this domain, other than the previous time history that led the system to the steady state under consideration. Accordingly, one should allow in principle any possible steady-state function of (H, μ) in this "trapped-electron" domain. We choose to write such trapped particle domain solution as

$$F_{2c} = F_0[H, \mu_c(H)] \, G[H, \mu - \mu_c(H)] \tag{38}$$

with $G(H, \bar{\mu})$ arbitrary. Once $F(\ell, H, \mu)$ is fully specified in all domains for a given $\phi(\boldsymbol{x})$,

equation (29) yields $n(\boldsymbol{x})$, which is implemented in the ion fluid model of next Section to provide a new $\phi(\boldsymbol{x})$, and iteration progresses until convergence is achieved to the self-consistent $\phi(\boldsymbol{x})$ and $n(\boldsymbol{x})$.

It turns out that the choice of $G(H, \bar{\mu})$ has a large impact in the solution for $n(\boldsymbol{x})$. The steady-state paraxial model of Ref. [31] assumed G to be a constant α, equal or lower than 1. Then, in the asymptotic downstream limit, where $B \to 0$ and $n \to 0$, the vanishing $n(\boldsymbol{x})$ was surprisingly dominated by trapped electrons instead of by free electrons. More recently, the paraxial model of Ref. [32] obtained numerically the time-dependent, initial-value solution of a related collisionless MN problem. Its long-time behavior is in agreement with the steady-state solution (35)-(38); the chosen initial conditions and the collisionless transient dynamics specify a particular form of the function $G(H, \bar{\mu})$, that vanishes at $\bar{\mu} \to \infty$ and reduces the relevance of trapped electrons far downstream.

A. Downstream asymptotic analysis

It is possible to study analytically the asymptotic behavior of the fluid moments of the steady-state solution (35)–(38) in the far downstream limit, even without knowing the self-consistent profile of $\phi(\ell)$. This analysis illustrates a number of important physical features in the divergent MN such as the plasma expansion laws, its anisotropic collisionless cooling, and the relevance there of trapped electrons (of phase-space domain $2c$).

For the sake of clarity, the analysis is particularized for an upstream Maxwellian reservoir, that is

$$F_0(H, \mu) = F_M(H) \equiv N_0 (2\pi T_{e0})^{-3/2} \exp\left(-H/T_{e0}\right) \tag{39}$$

and equations (29)–(31) assure that the constants N_0 and T_{e0} are indeed the far upstream density and temperature:

$$n(\ell \to -\infty) = N_0, \qquad p_{e\parallel}(\ell \to -\infty) = p_{e\perp}(\ell \to -\infty) = N_0 T_{e0}. \tag{40}$$

Far downstream, it is useful to show separately the contributions of the free-electron, reflected-electron and trapped-electron domains, which will be labeled respectively with the f, r and t superscripts. For $\ell \to +\infty$, where $\phi \to \phi_\infty$ and $B \to 0$, the asymptotic

contribution of the free-electron domain is

$$n^f(\ell \to +\infty) = \frac{N_0 B}{2\pi^{1/2} T_{e0}} \exp\left(\frac{e\phi_\infty}{T_{e0}}\right) \int_0^\infty \mathrm{d}t \exp(-t) t^{-1/2} \mu_c\left(T_{e0}t - e\phi_\infty\right), \qquad (41)$$

$$p_{e\parallel}^f(\ell \to +\infty) = \frac{N_0 B}{\pi^{1/2}} \exp\left(\frac{e\phi_\infty}{T_{e0}}\right) \int_0^\infty \mathrm{d}t \exp(-t) t^{1/2} \mu_c\left(T_{e0}t - e\phi_\infty\right), \qquad (42)$$

$$p_{e\perp}^f(\ell \to +\infty) = O(B^2) \ll p_{e\parallel}^f(\ell \to +\infty). \qquad (43)$$

This asymptotic behavior $(n^f \propto B, p_{e\parallel}^f \propto B, p_{e\perp}^f \propto B^2)$ is consistent with a double-adiabatic equation of state,

$$p_{e\parallel}^f \propto \frac{(n^f)^3}{B^2}, \qquad p_{e\perp}^f \propto n^f B. \qquad (44)$$

For $\ell \to +\infty$, where $\phi \to \phi_\infty$ and $B \to 0$, the asymptotic contribution of the reflected-electron domain is

$$n^r(\ell \to +\infty) = \frac{2N_0 B}{\pi^{1/2} T_{e0}} \left[\frac{e}{T_{e0}}(\phi - \phi_\infty)\right]^{1/2} \exp\left(\frac{e\phi_\infty}{T_{e0}}\right) \mu_c\left(-e\phi_\infty\right), \qquad (45)$$

$$p_{e\parallel}^r(\ell \to +\infty) = \frac{4N_0 B}{3\pi^{1/2}} \left[\frac{e}{T_{e0}}(\phi - \phi_\infty)\right]^{3/2} \exp\left(\frac{e\phi_\infty}{T_{e0}}\right) \mu_c\left(-e\phi_\infty\right), \qquad (46)$$

$$p_{e\perp}^r(\ell \to +\infty) = O\left[B^2(\phi - \phi_\infty)^{1/2}\right], \qquad (47)$$

which is also consistent with a double-adiabatic equation of state[42]

$$p_{e\parallel}^r \propto \frac{(n^r)^3}{B^2}, \qquad p_{e\perp}^r \propto n^r B, \qquad (48)$$

but is always negligible compared to the free-electron contribution (41)–(43).

Evaluating the contribution of the trapped-electron domain requires knowing the function $G(H, \bar{\mu})$ in equation (38) which, as discussed above, is not possible based on steady-state considerations alone. Here we shall consider two heuristic models for this function and explore the different outcomes that follow from such working assumptions. The first one (labeled as $t1$) assumes a constant $G(H, \bar{\mu}) = \alpha$ with $0 < \alpha \le 1$, meaning that the trapped electrons are thermalized and fill the whole range of available magnetic moments. This was the model adopted (with $\alpha = 1$) in [31] and yields

$$n^{t1}(\ell \to +\infty) = \alpha \frac{4N_0}{3\pi^{1/2}} \left[\frac{e}{T_{e0}}(\phi - \phi_\infty)\right]^{3/2} \exp\left(\frac{e\phi_\infty}{T_{e0}}\right) \qquad (49)$$

$$p_{e\parallel}^{t1}(\ell \to +\infty) = \alpha \frac{8N_0 T_{e0}}{15\pi^{1/2}} \left[\frac{e}{T_{e0}}(\phi - \phi_\infty)\right]^{5/2} \exp\left(\frac{e\phi_\infty}{T_{e0}}\right) \qquad (50)$$

$$p_{e\perp}^{t1}(\ell \to +\infty) = \alpha \frac{8N_0 T_{e0}}{15\pi^{1/2}} \left[\frac{e}{T_{e0}}(\phi - \phi_\infty)\right]^{5/2} \exp\left(\frac{e\phi_\infty}{T_{e0}}\right), \qquad (51)$$

consistent with an isotropic, adiabatic equation of state

$$p_{e\parallel}^{t1} = p_{e\perp}^{t1} \propto (n^{t1})^{5/3}. \tag{52}$$

The complete numerical solution of [31] showed a downstream asymptotic behavior of the electric potential $(\phi - \phi_\infty) \propto B^{2/3}$. In this case, the trapped-electron asymptotic contribution to the density is comparable to the free-electron one, $n^{t1} \propto B \sim n^f$, and the trapped-electron asymptotic contributions to the pressures are $p_{e\parallel}^{t1} \propto B^{5/3} \ll p_{e\parallel}^f$ and $p_{e\perp}^f \ll p_{e\perp}^{t1} \propto B^{5/3} \ll p_{e\parallel}^f$. Thus, the asymptotic behaviors of the parallel and perpendicular temperatures are

$$T_{e\parallel} \equiv \frac{p_{e\parallel}}{n} \to \frac{p_{e\parallel}^f}{n^f + n^{t1}} \to \text{constant} \tag{53}$$

and

$$T_{e\perp} \equiv \frac{p_{e\perp}}{n} \to \frac{p_{e\perp}^{t1}}{n^f + n^{t1}} \propto B^{2/3} \ll T_{e\parallel}. \tag{54}$$

Our second model for the steady-state trapped-electron distribution function (labeled as $t2$) is motivated by the initial-value, dynamical analysis of a related collisionless plasma model in Ref. [32]. This work showed a time-dependent electron distribution function that approaches a steady-state at long times, having the form given by equations (35)–(38) with a specific $F_{2c}(H, \mu)$. This distribution of trapped electrons was formed during the transient evolution and approaches the Maxwellian $F_M(H)$ at $\mu = \mu_c(H)$, making a continuous transition to the reflected-electron domain at the trapped-untrapped boundary. Then, it is a decreasing function of $\mu - \mu_c(H)$, that tends to zero away from such trapped-untrapped boundary. Accordingly, we postulate a $G(H, \bar{\mu})$ function satisfying $G(H, 0) = 1$ and

$$\int_0^\infty G(H, \bar{\mu}) \mathrm{d}\bar{\mu} = J(H) < \infty \tag{55}$$

so that

$$\lim_{\epsilon \to 0} \frac{1}{\epsilon} G\left(H, \frac{\bar{\mu}}{\epsilon}\right) = J(H)\delta(\bar{\mu}). \tag{56}$$

With this assumption, the trapped-electron asymptotic contribution in the far downstream limit, where $\phi \to \phi_\infty$ and $B \to 0$, is comparable to the reflected-electron contribution:

$$n^{t2}(\ell \to +\infty) = \frac{2N_0 B}{\pi^{1/2} T_{e0}} \left[\frac{e}{T_{e0}}(\phi - \phi_\infty)\right]^{1/2} \exp\left(\frac{e\phi_\infty}{T_{e0}}\right) J\left(-e\phi_\infty\right), \tag{57}$$

$$p_{e\parallel}^{t2}(\ell \to +\infty) = \frac{4N_0 B}{3\pi^{1/2}} \left[\frac{e}{T_{e0}}(\phi - \phi_\infty)\right]^{3/2} \exp\left(\frac{e\phi_\infty}{T_{e0}}\right) J\left(-e\phi_\infty\right), \tag{58}$$

$$p_{e\perp}^{t2}(\ell \to +\infty) = O\left[B^2(\phi - \phi_\infty)^{1/2}\right]. \tag{59}$$

This is now also consistent with a double-adiabatic equation of state,

$$p_{e\parallel}^{t2} \propto \frac{(n^{t2})^3}{B^2}, \qquad p_{e\perp}^{t2} \propto n^{t2}B, \tag{60}$$

and is negligible compared to the free-electron contribution. Finally, the asymptotic behaviors of the parallel and perpendicular temperatures in this case are

$$T_{e\parallel} \equiv \frac{p_{e\parallel}}{n} \to \frac{p_{e\parallel}^f}{n^f} \to \text{constant} \tag{61}$$

and

$$T_{e\perp} \equiv \frac{p_{e\perp}}{n} \to \frac{p_{e\perp}^f}{n^f} \propto B \ll T_{e\parallel}. \tag{62}$$

IV.   THREE-DIMENSIONAL SOLUTION SCHEME FOR THE ION FLUID SYSTEM

The drift-kinetic electron model is coupled with the fluid ion equations through the quasineutrality condition (6). The ion momentum equation (14) has the Bernoulli integral

$$\boldsymbol{u}_i \cdot \nabla \left(\frac{m_i}{2}|\boldsymbol{u}_i|^2 + e\phi \right) = 0. \tag{63}$$

Therefore, considering that the previous electron drift-kinetic model provides n, the ion fluid system (13)-(14) for ϕ and $\boldsymbol{u}_i$ can be written as

$$e\phi = m_i \left(\hat{h}_i - |\boldsymbol{u}_i|^2/2 \right) \qquad \text{with} \qquad \boldsymbol{u}_i \cdot \nabla \hat{h}_i = 0, \tag{64}$$

where $\hat{h}_i$ is the Bernouilli energy, constant along each ion flow line,

$$\boldsymbol{B} \cdot \nabla \left(\frac{n u_{i\parallel}}{B} \right) = -\nabla \cdot (n\boldsymbol{u}_{i\perp}), \tag{65}$$

$$\boldsymbol{u}_{i\perp} = \frac{m_i}{eB} \boldsymbol{b} \times \left[\nabla \hat{h}_i + (\nabla \times \boldsymbol{u}_i) \times \boldsymbol{u}_i \right]. \tag{66}$$

The solution of this system depends on the relative magnitude of the two small parameters $\rho_e/L \equiv m_e v_{the}/(eBL) \ll 1$ and $m_e/m_i \ll 1$, and two separate cases can be considered. The first corresponds to $\rho_e/L \ll (m_e/m_i)^{1/2}$, in which case the ion-sound-gyroradius ρ_S is much less than the scale length L:

$$\frac{\rho_S}{L} \equiv \frac{m_i c_S}{eBL} = \frac{(m_i m_e)^{1/2}v_{the}}{eBL} = \frac{\rho_e}{L} \left(\frac{m_i}{m_e} \right)^{1/2} \ll 1. \tag{67}$$

The second corresponds to $\rho_e/L \sim (m_e/m_i)^{1/2}$, in which case ρ_S is comparable to L:

$$\frac{\rho_S}{L} = \frac{\rho_e}{L} \left(\frac{m_i}{m_e} \right)^{1/2} \sim 1. \tag{68}$$

A. Small ion-sound-gyroradius

When $\rho_S/L \equiv m_i c_S/(eBL) \ll 1$, the cold ions are effectively magnetized and the ion parallel flow velocity is much greater than the perpendicular velocity:

$$u_{i\parallel} \sim c_S \gg |\boldsymbol{u}_{i\perp}| \simeq \frac{m_i}{eB}\left|\boldsymbol{b} \times \left[(\nabla \times u_{i\parallel}\boldsymbol{b}) \times u_{i\parallel}\boldsymbol{b}\right]\right| \sim \frac{\rho_S c_S}{L}. \tag{69}$$

Therefore, the ion continuity equation is

$$\boldsymbol{B} \cdot \nabla\left(\frac{n u_{i\parallel}}{B}\right) = -\nabla \cdot (n\boldsymbol{u}_{i\perp}) \sim \frac{n\rho_S c_S}{L^2} \ll \frac{n u_{i\parallel}}{L} \tag{70}$$

and its the leading-order solution is

$$u_{i\parallel} = \frac{k_i B}{n} \qquad \text{with} \qquad \boldsymbol{B} \cdot \nabla k_i = 0, \tag{71}$$

so that for each streamline k_i is the (constant) ratio of ion to magnetic flux. Retaining only this leading-order accuracy, the stream lines for the ion flow coincide with the magnetic field lines and the solution for the electric potential is

$$e\phi = m_i\left(\hat{h}_i - \frac{k_i^2 B^2}{2n^2}\right) \tag{72}$$

where both $\hat{h}_i$ and k_i are now constant along the magnetic field. Equation (72) provides a relationship between the density and the electric potential on each magnetic line which, coupled to the electric drift-kinetic system (27)–(31), allows to solve the three-dimensional problem one magnetic line at a time[35, 36]. In addition to the integration constants $\hat{h}_i$ and k_i, the behavior of the plasma solution on each different magnetic line depends only on the variation $B(\ell)$ of the magnitude of the magnetic field as a function of the arc length along the line, which is given by the chosen nozzle coil configuration. Calling $\phi(\ell \to +\infty) = \phi_\infty$, the downstream asymptotic behavior of the density and the ion velocity for $\ell \to +\infty$ are

$$u_{i\parallel} \to u_{i\parallel\infty} = \left(2\hat{h}_i - \frac{2e\phi_\infty}{m_i}\right)^{1/2}, \qquad n \to \frac{k_i B}{u_{i\parallel\infty}} \propto B. \tag{73}$$

Furthermore, if $u_{i\parallel}(\ell \to -\infty) \to 0$, then $\hat{h}_i = 0$ for all magnetic (and ion) lines, and several expressions above simplify.

B. Large ion-sound-gyroradius

When $\rho_S/L \equiv m_i c_S/(eBL) \sim 1$, the cold ions are partially demagnetized so that the parallel and perpendicular components of the ion flow velocity are comparable:

$$u_{i\parallel} \sim |\boldsymbol{u}_{i\perp}| = \frac{m_i}{eB} |\boldsymbol{b} \times [(\nabla \times \boldsymbol{u}_i) \times \boldsymbol{u}_i]| \sim \frac{\rho_S c_S}{L} \sim c_S. \tag{74}$$

In this case, the complete ion fluid system (64)–(66) must be solved in the whole three-dimensional space. This problem admits a notable simplification when $\hat{h}_i$ are the same for all the ion flow lines, as in the case where all ions have negligible velocity far upstream, $u_{i\parallel}(\ell \to -\infty) \to 0$. Under this assumption, we eliminate $u_{i\parallel}$ in favor of its renormalized counterpart

$$\lambda \equiv \frac{u_{i\parallel}}{\Omega_{ci} + \omega_{i\parallel}}, \tag{75}$$

where $\Omega_{ci} = eB/m_i$ is the ion cyclotron frequency and

$$\omega_{i\parallel} \equiv \boldsymbol{b} \cdot (\nabla \times \boldsymbol{u}_i) \tag{76}$$

is the parallel ion vorticity which, under the working assumption that the plasma current contribution to the magnetic field is negligible so that $\nabla \times \boldsymbol{B} = 0$ outside the coils, can also be expressed as

$$\omega_{i\parallel} = \frac{1}{B} \nabla \cdot (\boldsymbol{u}_{i\perp} \times \boldsymbol{B}). \tag{77}$$

Then, in terms of the variable λ, the ion perpendicular momentum equation (66) becomes

$$\boldsymbol{u}_{i\perp} + \lambda \omega_{i\parallel} \boldsymbol{b} - \lambda \nabla \times (\boldsymbol{u}_{i\perp} + \lambda \omega_{i\parallel} \boldsymbol{b}) = \Omega_{ci} \lambda \nabla \lambda \times \boldsymbol{b} \tag{78}$$

which, assuming λ to be a given input, is now a linear equation for $\boldsymbol{u}_{i\perp}$. Moreover, the ion continuity equation (65) reduces to the simpler form

$$\boldsymbol{u}_i \cdot \nabla(n\lambda) = 0. \tag{79}$$

The details of the derivation of the last two equations are given in Appendix A. Therefore, for $\hat{h}_i$ equal to a constant everywhere, the system of partially demagnetized ion equations for large ion-sound-gyroradius simplifies to

$$\lambda = \frac{m_i \hat{k}_i}{en} \qquad \text{with} \qquad \boldsymbol{u}_i \cdot \nabla \hat{k}_i = 0 \tag{80}$$

and

$$e\phi = m_i \left[\hat{h}_i - \frac{\hat{k}_i^2 B^2}{2n^2} \left(1 + \frac{\omega_{i\parallel}}{\Omega_{ci}} \right)^2 - \frac{|\boldsymbol{u}_{i\perp}|^2}{2} \right],$$ (81)

along with (77), (78) for $\omega_{i\parallel}$ and $\boldsymbol{u}_{i\perp}$, where both $\hat{h}_i$ and $\hat{k}_i$ are now constant along the ion streamline. Observe that the parallel flow velocity is given by

$$u_{i\parallel} = \frac{\hat{k}_i B}{n} \left(1 + \frac{\omega_{i\parallel}}{\Omega_{ci}} \right).$$ (82)

C.   Direct integration of ion equations

The method of solution presented above begins with a density guess $n(\boldsymbol{x})$ for the ion equations, from which an electric potential map $\phi(\boldsymbol{x})$ is then computed. This feeds the kinetic electron model, which yields its own density calculation. The density error with respect to the initial guess can then be used to establish an iterative convergence procedure.

An alternative scheme for integrating the ion model in the large ion-sound-gyroradius case relies on the direct integration of the ion equation of motion. Firstly, a potential $\phi(\boldsymbol{x})$ guess is produced, from where $\boldsymbol{E}(\boldsymbol{x}) = -\nabla\phi$ can be computed. For prescribed fields $\boldsymbol{B}(\boldsymbol{x})$, $\boldsymbol{E}(\boldsymbol{x})$, the cold ion momentum equation (14) has a single characteristic family, which coincides with the ion trajectories. The characteristic equation is solved from the upstream boundary condition, where n, $\boldsymbol{u}_i$ are assumed known. This procedure yields the ion velocity map in the MN, $\boldsymbol{u}_i(\boldsymbol{x})$:

$$\frac{\mathrm{d}\boldsymbol{u}_i}{\mathrm{d}s_i} = \frac{e_i}{m_i u_i} \left(\boldsymbol{E} + \boldsymbol{u}_i \times \boldsymbol{B} \right),$$ (83)

where s_i is the arc-length coordinate along ion trajectories. Secondly, the continuity equation (13) is used to compute $n(\boldsymbol{x})$,

$$\frac{\mathrm{d}\ln n}{\mathrm{d}s_i} = \frac{1}{u_i} \nabla \cdot \boldsymbol{u}_i.$$ (84)

This value of $n(\boldsymbol{x})$ is then compared against the output of the electron drift-kinetic model, equations (27)–(29) for that $\phi(\boldsymbol{x})$. Then, the density difference error in (6) (or alternatively, the Poisson equation on n_i, n_e) can be used to set up the iterative convergence scheme for the self-consistent solution $\phi(\boldsymbol{x})$, $\boldsymbol{u}_i$, n. As a side note, observe that in the small ion-sound-gyroradius limit this treatment of the ion equations coincides with the one given in Section IV A.

Incidentally, observe that, beyond the ion trajectories, two additional Mach characteristic families are present in the two-fluid model of [26] when a simple relation $\phi = \phi(n)$, based in an heuristic closure of electron equations, is used.

V. ELECTRON FLUID EQUATIONS AND THE LOW PLASMA CURRENT CONDITION

The electron fluid system of (15) and the perpendicular components of (16) is to be solved as a post-process, once the density and the electron pressure tensor are known from the solution of the coupled ion-fluid and electron-drift-kinetic systems. Accordingly, the electron perpendicular velocity is given explicitly by

$$\boldsymbol{u}_{e\perp} = \frac{1}{B}\boldsymbol{b} \times \left(\nabla\phi - \frac{1}{en}\nabla \cdot \mathsf{P}_e\right) = \boldsymbol{b} \times \left(\frac{\nabla\phi}{B} - \frac{\nabla p_{e\perp} + (p_{e\parallel} - p_{e\perp})\boldsymbol{\kappa}}{enB}\right) \tag{85}$$

with $\boldsymbol{\kappa} = \boldsymbol{b} \cdot \nabla\boldsymbol{b}$ the magnetic curvature. The electron flow perpendicular velocity combines the $\boldsymbol{E} \times \boldsymbol{B}$ and the pressure gradient contributions and its order of magnitude is

$$|\boldsymbol{u}_{e\perp}| \sim \frac{T_e}{eBL} \sim \frac{\rho_S c_S}{L}. \tag{86}$$

Then, the electron parallel velocity follows from the continuity equation

$$\boldsymbol{B} \cdot \nabla\left(\frac{nu_{e\parallel}}{B}\right) = -\nabla \cdot (n\boldsymbol{u}_{e\perp}) \sim \frac{n\rho_S c_S}{L^2}. \tag{87}$$

Again, in the low ion-sound gyroradius limit, this equation reduces in leading order to

$$u_{e\parallel} = \frac{k_e B}{n} \qquad \text{with} \qquad \boldsymbol{B} \cdot \nabla k_e = 0. \tag{88}$$

Notice that the development of pressure anisotropy in the kinetic formulation of electrons prevents postulating the existence of a barotropic function h_e (defined by $\nabla h_e = \nabla p_e/n_e$) and a thermalized potential $\phi^* = \phi - h_e/e$, which were very useful in electron fluid models of Refs. [26, 36] to reduce the electron momentum equations (33) and (85) to simple expressions.

Throughout this work it is assumed that the contribution of the plasma current to the magnetic field is negligible, so the magnetic field is a fixed input, specified solely by the applied currents in the hardwired coils. For this to be valid, the condition $en|\boldsymbol{u}_i - \boldsymbol{u}_e| \ll B/L$ must be satisfied. The perpendicular flows are $|\boldsymbol{u}_{i,e\perp}| \sim \rho_S c_S/L$ hence the low-beta

assumption, $\beta_e \equiv nT_e/B^2 \ll 1$, guarantees that the perpendicular component of the plasma current is sufficiently small:

$$en|\boldsymbol{u}_{i\perp} - \boldsymbol{u}_{e\perp}| \sim \frac{en\rho_S c_S}{L} = \frac{nT_e}{BL} = \beta_e \frac{B}{L} \ll \frac{B}{L}. \tag{89}$$

From equations (65), (87), the parallel flows are

$$u_{i,e\parallel} = \frac{k_{i,e}B}{n} + O\left(\frac{\rho_S c_S}{L}\right) = O(c_S) + O\left(\frac{\rho_S c_S}{L}\right), \qquad \text{with } \boldsymbol{B}\cdot\nabla k_{i,e} = 0. \tag{90}$$

In the large ion-sound-gyroradius case, $\rho_S/L \sim 1$, the low-beta assumption also guarantees a sufficiently small parallel plasma current:

$$en(u_{i\parallel} - u_{e\parallel}) \sim enc_S \sim \frac{en\rho_S c_S}{L} = \beta_e \frac{B}{L} \ll \frac{B}{L}. \tag{91}$$

However, in the small ion-sound-gyroradius case, $\rho_S/L \ll 1$, we have

$$en(u_{i\parallel} - u_{e\parallel}) = eB(k_i - k_e) + O\left(\beta_e \frac{B}{L}\right) \tag{92}$$

so, in addition to $\beta_e \ll 1$, it is necessary to enforce the independent condition $eL(k_i - k_e) \ll 1$. Observe that when $\beta_e \sim 1$ the plasma-induced magnetic field is comparable to the applied one, and can thus modify the geometry of the magnetic nozzle. The study of the plasma-induced magnetic field can be approached setting up an iterative convergence method on top of the kinetic-fluid model, in the same way as in [40].

VI.   SUMMARY AND CONCLUDING REMARKS

A three-dimensional fluid-kinetic model of a collisionless plasma channeled and acceler-ated by a convergent-divergent MN has been formulated. The model provides a consistent collisionless solution for each species to dominant orders of each variable and for plausible plasma conditions: quasineutrality, small electron gyroradius, low plasma-beta, negligible electron inertia, and cold ions. Ion and electron velocities are of the order the ion sound velocity. The model provides the self-consistent electron thermodynamics in the plasma plume, enables the study of non-Maxwellian and non-isotropic electron populations, rele-vant in devices like the ECRT.

The kinetic part of the model determines at each magnetic line the zeroth-order electron VDF for a given (monotonically decreasing) electric potential profile. Then, the plasma

density and parallel and perpendicular pressures are obtained by integral moments of the VDF. The fluid part of the model provides the rest of magnitudes: electric potential, ion velocities, and electron velocities. The two parts of the model are coupled through the electric potential (or equivalently, through the plasma density). The computation of the electron velocities can be carried out separately at the end.

An asymptotic study of the far-downstream behavior of the different electron populations (free, reflected, trapped) in the kinetic model has been carried out, showing different adiabatic, anisotropic laws, and pointing out the limitations of this stationary model on defining the trapped electron population. The downstream pressure anisotropy also indicates that the polytropic law closure, based on an isotropic pressure, postulated in the fluid DIMAGNO and FUMAGNO models is not fully consistent.

There are two well distinguished cases of the ion fluid model depending on ion magnetization. For the small the ion-sound gyroradius case (i.e. ion full-magnetization), ion fluid equations can be solved independently at each magnetic line, so the 3D problem reduces to a set of infinite one-dimensional (1D) problems. This problem was already solved, with a slightly different formulation, for the central line of a paraxial (i.e. quasi 1D) MN [31], showing that convergence of the fluid and kinetic parts is achievable. The numerical implementation to 2D and 3D geometries should not present big difficulties.

Then, there is the large ion-sound gyroradius case, with ions partially or totally demagnetized, such that ion lines are not following magnetic lines. This is indeed the most interesting case, since in current applications the small ion-sound gyroradius case applies, at most, within a limited region around the MN throat, where the magnetic field is maximum. In particular, the demagnetization of ions and subsequent beam detachment in the MN downstream side is a central aspect of its physics. The implementation of a numerical scheme for the large the ion-sound gyroradius case is still pending, even for a 2D axisymmetric geometry. The advantageous three-characteristics scheme used in DIMAGNO[26] cannot be extended to the present ion model due to the coupling with the electron kinetic equation and the 3D geometry. This paper limits itself to suggest two possible forms of integrating the ion equations, leading to two different numerical schemes, leaving for further work the investigation of these last ones.

Finally, the numerical implementation will also have to deal with the expected univocal relation between the total electric potential fall along the nozzle, $|\phi_\infty|$, and the electric

current carried by the beam [31]; in particular there should be a single $|\phi_\infty|$ for a current-free beam. If this last condition is imposed and $|\phi_\infty|$ is an unknown of the problem, a second iteration loop appears in solving consistently the problem.

Appendix A: Large ion-sound-gyroradius ion equations

This Appendix details the derivation of the ion fluid results for large ion-sound-gyroradius used in Section IV B. When $\nabla(m_i u_i^2/2 + e\phi) = 0$, the perpendicular ion momentum equation (66) reduces to

$$\boldsymbol{u}_{i\perp} = \frac{1}{\Omega_{ci}}\boldsymbol{b} \times [(\nabla \times \boldsymbol{u}_i) \times \boldsymbol{u}_i)] = \frac{1}{\Omega_{ci}}[u_{i\parallel}(\nabla \times \boldsymbol{u}_i) - \omega_{i\parallel}\boldsymbol{u}_i)] \tag{A1}$$

where $\Omega_{ci} = eB/m_i$ is the ion cyclotron frequency and $\omega_{i\parallel} = \boldsymbol{b} \cdot (\nabla \times \boldsymbol{u}_i)$ is the parallel ion vorticity. This can be rewritten as

$$(\Omega_{ci} + \omega_{i\parallel})\boldsymbol{u}_{i\perp} = u_{i\parallel}(\nabla \times \boldsymbol{u}_i - \omega_{i\parallel}\boldsymbol{b}) \tag{A2}$$

and, introducing the variable $\lambda = u_{i\parallel}/(\Omega_{ci} + \omega_{i\parallel})$,

$$\boldsymbol{u}_{i\perp} = \lambda(\nabla \times \boldsymbol{u}_i - \omega_{i\parallel}\boldsymbol{b}). \tag{A3}$$

Eliminating now $u_{i\parallel}$ in favor of λ one arrives at

$$\boldsymbol{u}_{i\perp} = \lambda\left\{\nabla \times [\boldsymbol{u}_{i\perp} + \lambda(\Omega_{ci} + \omega_{i\parallel})\boldsymbol{b}] - \omega_{i\parallel}\boldsymbol{b}\right\} \tag{A4}$$

which, using the condition $\nabla \times \boldsymbol{B} = 0$, becomes the result of (78)

$$\boldsymbol{u}_{i\perp} = \lambda\left[\nabla \times \left(\boldsymbol{u}_{i\perp} + \lambda\omega_{i\parallel}\boldsymbol{b}\right) + \Omega_{ci}\nabla\lambda \times \boldsymbol{b} - \omega_{i\parallel}\boldsymbol{b}\right]. \tag{A5}$$

From (A3) and $\nabla \cdot \boldsymbol{B} = 0$, one obtains

$$\nabla \cdot \left(\frac{\boldsymbol{u}_{i\perp}}{\lambda}\right) = -\boldsymbol{B} \cdot \nabla\left(\frac{\omega_{i\parallel}}{B}\right) \tag{A6}$$

hence

$$\lambda \nabla \cdot \boldsymbol{u}_{i\perp} = \boldsymbol{u}_{i\perp} \cdot \nabla \lambda + \lambda^2 \nabla \cdot \left(\frac{\boldsymbol{u}_{i\perp}}{\lambda}\right) = \boldsymbol{u}_{i\perp} \cdot \nabla \lambda - \lambda^2 \boldsymbol{B} \cdot \nabla \left(\frac{\omega_{i\parallel}}{B}\right). \tag{A7}$$

On the other hand,

$$\lambda \nabla \cdot (u_{i\parallel}\boldsymbol{b}) = \lambda \boldsymbol{B} \cdot \nabla \left(\frac{u_{i\parallel}}{B}\right) = u_{i\parallel}\boldsymbol{b} \cdot \nabla \lambda + \lambda^2 \boldsymbol{B} \cdot \nabla \left(\frac{u_{i\parallel}}{B\lambda}\right) \tag{A8}$$

and the definition of λ implies

$$\frac{u_{i\parallel}}{B\lambda} = \frac{\omega_{i\parallel}}{B} + \frac{e}{m_i} \tag{A9}$$

so that

$$\lambda \nabla \cdot (u_{i\parallel}\boldsymbol{b}) = u_{i\parallel}\boldsymbol{b} \cdot \nabla \lambda + \lambda^2 \boldsymbol{B} \cdot \nabla \left(\frac{\omega_{i\parallel}}{B}\right). \tag{A10}$$

Then, the sum of (A7) and (A10) yields

$$\lambda \nabla \cdot \boldsymbol{u}_i = \boldsymbol{u}_i \cdot \nabla \lambda \tag{A11}$$

which, combined with the continuity equation $\nabla \cdot (n\boldsymbol{u}_i) = 0$, yields the result of equation (79),

$$\boldsymbol{u}_i \cdot \nabla(n\lambda) = 0. \tag{A12}$$

---

[1] S.A. Andersen, V.O. Jensen, P. Nielsen, and N. D'Angelo. Continuous supersonic plasma wind tunnel. *Phys. Fluids*, 12(3):557–560, 1969.

[2] K. Kuriki and O. Okada. Experimental study of a plasma flow in a magnetic nozzle. *Physics of Fluids*, 13(9):2262, 1970.

[3] R.A. Gerwin, G.J. Marklin, A.G. Sgro, and A.H. Glasser. Characterization of plasma flow through magnetic nozzles. Technical Report AFSOR AL-TR-89-092, Los Alamos National Laboratory, 1990.

[4] Eduardo Ahedo. Plasmas for space propulsion. *Plasma Physics and Controlled Fusion*, 53(12):124037, 2011. URL: http://stacks.iop.org/0741-3335/53/i=12/a=124037.

[5] Mario Merino and Eduardo Ahedo. Magnetic nozzles for space plasma thrusters. In J. Leon Shohet, editor, *Encyclopedia of Plasma Technology*, volume 2, pages 1329–1351. Taylor and Francis, 2016.

[6] C. Charles, R. Boswell, and M.A. Lieberman. Xenon ion beam characterization in a helicon double layer thruster. *Applied Physics Letters*, 89(26):261503, 2006.

[7] F.F. Chen. Permanent magnet helicon source for ion propulsion. *Plasma Science, IEEE Transactions on*, 36(5):2095–2110, 2008.

[8] J. Prager, R. Winglee, T. Ziemba, B. Roberson, and G. Quetin. Ion energy characteristics downstream of a high power helicon. *Plasma Sources Science and Technology*, 17:025003, 2008.

[9] O.V. Batishchev. Minihelicon plasma thruster. *IEEE Transaction on Plasma Science*, 37(8):1563–1571, 2009.

[10] D. Pavarin, F. Ferri, M. Manente, D. Curreli, Y. Guclu, D. Melazzi, D. Rondini, S. Suman, J. Carlsson, C. Bramanti, E. Ahedo, V. Lancellotti, K. Katsonis, and G. Markelov. Design of 50W helicon plasma thruster. In *31th International Electric Propulsion Conference*, IEPC 2009-205, 2009.

[11] K. Takahashi, C. Charles, R. Boswell, W. Cox, and R. Hatakeyama. Transport of energetic electrons in a magnetically expanding helicon double layer plasma. *Applied Physics Letters*, 94(19):191503, 2009.

[12] Shunjiro Shinohara, Hiroyuki Nishida, Takao Tanikawa, Tohru Hada, Ikkoh Funaki, and Konstantin P Shamrai. Development of electrodeless plasma thrusters with high-density helicon plasma sources. *IEEE Transactions on Plasma Science*, 42(5):1245–1254, 2014.

[13] Mario Merino, Jaume Navarro, Eduardo Ahedo, Victor Gómez, Víctor Sánchez, Mercedes Ruiz, Käthe Dannenmayer, Eduard Bosch, and José González. Maiden tests of the HPT05 helicon plasma thruster prototype. In *Space Propulsion Conference 2016*, number 3125014, Rome, Italy, 2016. European Space Agency.

[14] J. Navarro-Cavallé, M. Wijnen, P. Fajardo, and E. Ahedo. Experimental characterization of a 1 kW helicon plasma thruster. *Vacuum*, 149:69 – 73, 2018. doi:https://doi.org/10.1016/j.vacuum.2017.11.036.

[15] Joel C Sercel. Electron-cyclotron-resonance (ECR) plasma acceleration. In *AIAA 19th Fluid Dynamics, Plasma Dynamics and Lasers Conference*, 1987.

[16] T Lafleur, F Cannat, J Jarrige, PQ Elias, and D Packan. Electron dynamics and ion acceleration in expanding-plasma thrusters. *Plasma Sources Science and Technology*, 24(6):065013, 2015.

[17] Julien Jarrige, S Correyero-Plaza, Paul-Quentin Elias, and Denis Packan. Investigation on the ion velocity distribution in the magnetic nozzle of an ecr plasma thruster using lif measurements. In *35th International Electric Propulsion Conference*, number IEPC-2017-382, 2017.

[18] V.B. Tikhonov, S.A. Semenikhin, J.R. Brophy, and J.E. Polk. Performance of 130kW MPD thruster with an external magnetic field and Li as a propellant. In *Proceedings of the 25 th International Electric Propulsion Conference*, pages 728–733, 1997.

[19] R.M. Myers. Geometric scaling of applied-field magnetoplasmadynamic thrusters. *Journal of Propulsion and Power*, 11(2), 1995.

[20] G. Krülle, M. Auweter-Kurtz, and A. Sasoh. Technology and application aspects of applied field magnetoplasmadynamic propulsion. *J. Propulsion and Power*, 14(5):754–763, 1998.

[21] R Albertoni, P Rossetti, F Paganucci, M Andrenucci, M Zuin, E Martinez, and R Cavazzana. Experimental study of a 100-kW-class applied-field MPD thruster. IEPC-2011-110, 32nd International Electric Propulsion Conference, Wiesbaden, Germany, 2011.

[22] Adam Boxberger, Patrick Bambach, Georg Herdrich, Stefanos Fasoulas, Mario Merino, and Eduardo Ahedo. Experimental investigation of applied-field magnetoplasmadynamic thrusters at institute of space systems. In 48th *AIAA/ASME/SAE/ASEE Joint Propulsion Conference & Exhibit*, number AIAA-2012-4012, Washington DC, 2012. AIAA. doi:10.2514/MJPC12.

[23] F. Chang-Diaz. The VASIMR rocket. *Scientific American*, 283(5):90–97, 2000.

[24] B.W. Longmier, E.A. Bering, M.D. Carter, L.D. Cassady, W.J. Chancery, F.R.C. Díaz, T.W. Glover, N. Hershkowitz, A.V. Ilin, G.E. McCaskill, et al. Ambipolar ion acceleration in an expanding magnetic nozzle. *Plasma Sources Science and Technology*, 20:015007, 2011.

[25] C.S. Olsen, M.G. Ballenger, M.D. Carter, F.R. Chang Diaz, M. Giambusso, T.W. Glover, A.V. Ilin, J.P. Squire, B.W. Longmier, E.A. Bering, and P.A. Cloutier. Investigation of plasma detachment from a magnetic nozzle in the plume of the vx-200 magnetoplasma thruster. *Plasma Science, IEEE Transactions on*, 43(1):252–268, 2015. doi:10.1109/TPS.2014.2321257.

[26] Eduardo Ahedo and Mario Merino. Two-dimensional supersonic plasma acceleration in a magnetic nozzle. *Physics of Plasmas*, 17(7):073501, 2010. doi:10.1063/1.3442736.

[27] J.J. Ramos. Fluid formalism for collisionless magnetized plasmas. *Physics of Plasmas*, 12(5):052102, 2005.

[28] Mario Merino and Eduardo Ahedo. Influence of electron and ion thermodynamics on the magnetic nozzle plasma expansion. *IEEE Transactions on Plasma Science*, 43(1):244–251, Jan 2015. `doi:10.1109/TPS.2014.2316020`.

[29] Yunchao Zhang, Christine Charles, and Rod Boswell. Thermodynamic study on plasma expansion along a divergent magnetic field. *Physical review letters*, 116(2):025001, 2016.

[30] JM Little and EY Choueiri. Electron cooling in a magnetically expanding plasma. *Physical Review Letters*, 117(22):225003, 2016.

[31] M Martinez-Sanchez, J Navarro-Cavallé, and E Ahedo. Electron cooling and finite potential drop in a magnetized plasma expansion. *Physics of Plasmas*, 22(5):053501, 2015.

[32] Gonzalo Sanchez-Arriaga, Jiewei Zhou, Eduardo Ahedo, Manuel Martinez-Sanchez, and Jesus Ramos. Kinetic features and non-stationary electron trapping in paraxial magnetic nozzles. *Plasma Sources Science and Technology*, 27(3):035002, 2018.

[33] Eduardo Ahedo and Mario Merino. On plasma detachment in propulsive magnetic nozzles. *Physics of Plasmas*, 18(5):053504, 2011. `doi:10.1063/1.3589268`.

[34] Mario Merino and Eduardo Ahedo. Plasma detachment in a propulsive magnetic nozzle via ion demagnetization. *Plasma Sources Science and Technology*, 23(3):032001, 2014. `doi:10.1088/0963-0252/23/3/032001`.

[35] Mario Merino and Eduardo Ahedo. Contactless steering of a plasma jet with a 3D magnetic nozzle. *Plasma Sources Science and Technology*, 26(9):095001, 2017. `doi:10.1088/1361-6595/aa8061`.

[36] Mario Merino and Eduardo Ahedo. Fully magnetized plasma flow in a magnetic nozzle. *Physics of Plasmas*, 23(2):023506, 2016. `doi:10.1063/1.4941975`.

[37] Mario Merino. Fumagno code: Fully-magnetized magnetic nozzle simulator, 2017. `doi:10.5281/zenodo.593787`.

[38] Eduardo Ahedo and Mario Merino. Two-dimensional plasma expansion in a magnetic nozzle: separation due to electron inertia. *Physics of Plasmas*, 19(8):083501, 2012. `doi:10.1063/1.4739791`.

[39] Mario Merino and Eduardo Ahedo. Two-dimensional quasi-double-layers in two-electron-temperature, current-free plasmas. *Physics of Plasmas*, 20(2):023502, 2013. `doi:10.1063/1.`

4789900.

[40] Mario Merino and Eduardo Ahedo. Effect of the plasma-induced magnetic field on a magnetic nozzle. *Plasma Sources Science and Technology*, 25(4):045012, 2016. doi:10.1088/0963-0252/25/4/045012.

[41] Mario Merino, Javier Mauriño, and Eduardo Ahedo. Kinetic electron model for plasma thruster plumes. *Plasma Sources Science and Technology*, (in press), 2018.

[42] G.F. Chew, M.L. Goldberger, and F.E. Low. The boltzmann equation and the one-fluid hydromagnetic equations in the absence of particle collisions. *Proceedings of the Royal Society of London*, A236:112–118, 1956.

[43] J.J. Ramos. Finite-larmor-radius kinetic theory of a magnetized plasma in the macroscopic flow reference frame. *Physics of plasmas*, 15:082106, 2008.